Microstructural evolution, fracture behavior and bonding mechanisms study of copper sintering on bare DBC substrate for SiC power electronics packaging

Liu, Xu; Li, Shizhen; Fan, Jiajie; Jiang, Jing; Liu, Yang; Ye, Huaiyu; Zhang, Guoqi

DOI
10.1016/j.jmrt.2022.05.122

Publication date
2022

Document Version
Final published version

Published in
Journal of Materials Research and Technology

Available online at www.sciencedirect.com

jmr&t Journal of Materials Research and Technology

journal homepage: www.elsevier.com/locate/jmrt

Original Article

Microstructural evolution, fracture behavior and bonding mechanisms study of copper sintering on bare DBC substrate for SiC power electronics packaging

Xu Liu [a,b,1], Shizhen Li [b,1], Jiajie Fan [c], Jing Jiang [c], Yang Liu [d], Huaiyu Ye [a,b,e,*], Guoqi Zhang [a,**]

[a] Department of Microelectronics, Delft University of Technology, 2628 CD Delft, the Netherlands
[b] School of Microelectronics, Southern University of Science and Technology, Shenzhen 518055, China
[c] Academy for Engineering & Technology, Fudan University, Shanghai 200433, China
[d] School of Material Science and Engineering, Harbin University of Science and Technology, Harbin, 150040, China
[e] The Key Laboratory of Optoelectronic Technology &Systems, College of Optoelectronic Engineering, Education Ministry of China, Chongqing University, Chongqing 400044, China

ARTICLE INFO

Article history:
Received 13 April 2022
Accepted 20 May 2022
Available online 27 May 2022

Keywords:
Sintered Cu
Shear strength
Microstructural evolution
Failure mechanism
SiC MOSFET packaging

ABSTRACT

Robust bonding of Cu quasi-nanoparticles sintering for Ag coated chip and bare copper substrate was achieved. The effect of temperature, pressure and time on the sintering bonding strength and microstructural evolution was deeply studied. 36.5 MPa shear strength was achieved when applied 5 MPa pressure. By increasing to 30 MPa, it shows the best die shear strength of 116 MPa, accomplished with a sintering temperature of 250 °C for 3 min. Temperature also influenced the shear strength a lot. Between 210 °C and 230 °C can already provide strength over 30 MPa. When increased to 270 °C, the strength was extremely enhanced to over 120 MPa. Inspection on the fracture behaviors and cross-section of sheared off samples was conducted by SEM, EDS, and XRD. It is found that low bonding performance is due to both of the incomplete burnt out of organics and incomplete Cu QNPs sintering. In addition, high bonding is account for the positive effect of pressure and temperature on promoting the necking growth, sintering networking formation, pores isolation and brittle-ductile fracture transformation. The recommended sintering profile is 250 °C, 3 min, 20 MPa. Finally, the feasibility for SiC MOSFET power electronics DA was verified by testing its static characteristics at both room temperature and 150 °C.

* Corresponding author.
** Corresponding author.
E-mail addresses: yehy@sustech.edu.cn (H. Ye), g.q.zhang@tudelft.nl (G. Zhang).
[1] These authors contributed equally to this work.

https://doi.org/10.1016/j.jmrt.2022.05.122

1. Introduction

Power electronics (PE) have been widely used in high-speed rail transportation, electric vehicles, 5G network and industrial motors for energy conversion and controlling [1,2]. In these applications, the reliable operation of semiconductor devices at high temperature is of great significance. Recently wide-bandgap (WBG) semiconductors materials, such as silicon carbide (SiC) and gallium nitride (GaN) were more and more applied due to their outstanding electrical, thermal and mechanical properties. However, conventional Pb-free solder joint materials such as Sn–Ag–Cu alloys with reflow temperature of 220–260 °C is not suitable at application temperatures higher than 200 °C due to their low remelting temperature and poor reliability. Therefore, there is an urgent need to develop new type of bonding materials, which can ensure excellent performance for higher operating temperature and higher power density raised by WBG semiconductors [3].

Nano-silver sintering [3–10] and transient liquid phase soldering (TLSP) method [11–13] have emerged as promising alternative bonding techniques for high temperature applications. However, these techniques possess inevitable drawbacks such as formation of brittle intermetallic compounds (IMC), risk of electro-chemical migration (ECM) and high material costs, which limit the largescale application in the future. Recently, nano copper sintering is receiving great attentions because of its much lower material cost (about 1–10% of the Ag price), lower ion migration tendency, as well as sufficiently high thermal conductivity (398 W/mK for bulk material) [14–18]. However, for the industrial application, the biggest challenges that nano copper material encountered are the high oxidation risk, high agglomeration tendency, higher sintering temperature and complex sintering process [6,19]. To solve these problems, different methods have been attempted. First of all, the most effective way to avoid copper oxidation and guarantee good bonding performance is injecting reducing atmosphere with specific concentration during sintering [20,21]. The similar scheme also includes setting an intentional oxidation-reduction process of copper NPs during the sintering [6,22–24]. However, from the industrial/practical application perspective, the reducing gas and oxidation-reduction reaction may increase the process cost as well as the complexity. For this reason, a protective treatment for Cu nano particles (NPs) in advance combined with applying of inert atmosphere during sintering can be a better way [25]. Different Cu NPs synthesis methods were proposed to obtain small-size NPs with low-temperature sintering ability and stable properties. Most of synthesis methods are based on the modified polyol method applying different precursor and reducing agent, such as hydrazine [26,27], citric acid [26], PVP [28,29], L-ascorbic acid [30,31], formic acid [32]. However, the above-mentioned methods heavily rely on the precise control of additives (polymers and surfactants) amount to control the diameter and prevent aggregation of Cu NPs in organic solvents simultaneously. Therefore, for the industrial scale applications such in-situ coating during the Cu NPs generating process is problematic. Accordingly, creating protective capping after the copper nano particle synthesis could be a more feasible solution. Liu et al. [33,34] used formic acid to treat the as-produced Cu NPs. Compared with the untreated Cu NPs, the treated Cu material shows better bonding strength (43.4 MPa) after sintering at 260 °C in H_2/N_2 mixing atmosphere with 10 MPa assisted pressure. To further reduce the oxidation risk during sintering, the sintering process should be as short as possible so that the copper material will not be exposed to the oxygen for too long. Hence, the most effective method to shorten the process time is to employ a moderate external pressure during the die attachment (DA) [25,29,30,32–34]. Gao et al. [35] used ascorbic acid to treat the as-produced NPs, and the produced NPs obtained the self-reductive ability. After sintering at 250 °C for 30 min with 0.4 MPa the joint showed over 15 MPa bonding strength. Zhao et al. [36] synthesized 30 nm mono-dispersed copper NPs and then did special treatment on them. The as treated copper paste could have 17 MPa shear strength after sintering at 240 °C. Even though, the reduction of Ag and Cu particle size could effectively lower the sintering temperature, pressure and process time to obtain the densified sintered joint [34,36,37], it can also increase the risk of particle spontaneous oxidation and agglomeration [38]. Applying Cu quasi-nanoparticles (QNPs, average diameter is between 100 nm and 200 nm) could be an alternative option [25,39,40]. In our previous researches [41,42], it was found that, via proper particle treatment, the particle with around 100 nm size could already be sintered well. Mou et al. [25] reported that they used carboxylic acid (formic acid and oxalic acid) to modify the surface of Cu NPs(150–200 nm) and they obtained over 20 MPa bonding performance by sintering at 250 °C for 60 min in $Ar–H_2$ (5% H_2) with 10 MPa assisted pressure.

In past few years, thanks to the development of pressure-assisted sintering machine (or so-called sintering press), it is possible to provide precise pressure control to multiple samples at the same time. Therefore, fast sintering process (less than 5 min per batch) is achieved in the industry. In order to ensure the sintering performance in such short time, it is first necessary to study the effect of process parameters on microstructural evolution and bonding mechanism. In the field of Ag sintering, there are plenty of researches on the impact of sintering process parameters [43–46]. However, for copper sintering the relative study is rare. In this work, the mass-production available Cu QNPs were applied to carry out the study. Cu QNPs reductive pre-treatment was conducted and reducing additives was blended to prepare a reductive copper paste. Then an in-depth study on the effect of temperature, pressure and time on the sintering joint bonding strength and sintering microstructural evolution was carried out. The relevant sintering joint neck formation, pores development and fracture surface were investigated. The sintering mechanism was obtained along with the optimized sintering process parameters which can be used in the practical application. Finally, the feasibility of the nano copper sintering as the real DA material for SiC MOSFET power electronics devices was verified by testing its static characteristics at both room temperature and 150 °C.

2. Material process and tests

2.1. Cu particles and others

In this study, the Cu quasi-nanoparticles (QNPs) used were synthesized by physical vapor deposition (PVD) methods. Fig. 1a and 1b shows the SEM morphology and TEM photos of copper particles after treatment. From Fig. 1a, it can be observed that Cu QNPs are quasi-spherical and uniformly mixed. The average particle diameter is around 150 nm and 300 nm. The detailed information of size distribution characterization will be discussed in next section. Fig. 1b shows that after treatment, there was a coating layer formed with nanometers thickness. Carboxylic acids A (99.0%), terpinol (95%), ethylene glycol (99.5%), and ethanol (99.7%) were purchased from Aladdin reagent Co., Ltd. The direct bonded copper (DBC) substrates and active metal brazing) (AMB) substrates with 38 mm × 27 mm size were purchased from Ferrotec. The thickness of Al_2O_3 layer is 0.38 mm and the thickness of upper and bottom copper plate are both 0.3 mm. A 3 mm × 3 mm × 1 mm oxide free copper (OFC) small plate with 2 μm Ag metallization surface coating was used as the dummy die.

2.2. Cu QNPs treatment and paste formulation

Then a reductive pretreatment was conducted to the QNPs in advance. 1 portion of reductive agent carboxylic acids A were dissolved into 500 mL absolute ethyl alcohol by magnetic stirring to prepare treating solution B. Then 50 g copper QNPs were added into solution B under continuous agitation. The treatment reaction was conducted at room temperature for 40 min till the color of solution changed to dark red (solution C). Then the solution C was centrifuged at 4000 rpm for 5 min, and washed 3 times by absolute ethyl alcohol to remove unreacted reactants. The obtained composite particles were heat-treated at 55 °C for 8 h in vacuum to obtain final composite QNPs. Then the as-treated QNPs (77 wt.%) were mixed with ethylene glycol (EG) and terpilenol with 1:1 ratio at 2000 rpm for 10 min through a mechanical blender to form a paste. Finally, the as-milled paste was further homogenized by the planet agitator at 1500 rpm for 2 min to form the final paste.

2.3. Sintering and tests

The morphology of Cu QNPs was observed by a field-emission scanning electron microscope (SEM, Zeiss GeminiSEM 300) and transmission electron microscopy (TEM, FEI Tecnai G2 F30). Then, the size distribution of Cu QNPs was measured and calculated by further analyzing the SEM photos. The X-ray diffraction (XRD) patterns were obtained by using an X-ray diffractometer (Rigaku Smartlab) with monochromated Cu Kα radiation (λ = 1.54 A). Thermogravimetric analysis (TGA) was conducted by using simultaneous thermogravimetry – differential scanning calorimetry (STA 449 F1 Jupiter) from room temperature (25 °C) to 600 °C with a ramping rate of 10 °C/min, under N_2 atmospheres.

In this research, there was a sandwich-like structure (dummy die/sintering layer/substrate) of Cu sintering joint samples being applied for shear strength test. As depicted in Fig. 2, first the copper paste was printed onto a DBC substrate forming six 5 mm × 5 mm × 100 μm sized patterns. Next, the substrates were delivered into a vacuum oven for drying process at 120 °C for 5 min to remove the organic solvent. Then six copper dummy die were placed onto the as-dried copper pad by using pick & place machine (Tresky T3002 PRO) with 0.5 MPa pressure. Finally, pressure-assisted sintering was conducted in nitrogen atmosphere using the industrial standard sintering machine (Boschman Sinterstar Mini). The built-in dynamic pressing tool could precisely control the sintering temperature (230–270 °C), sintering time (1–4 min) and sintering pressure (5–30 MPa). The design of experiment (DOE) in this study is shown in Table 1. Moreover, to check the bonding strength of the sintering joint, five bonded dummy die were sheared off by using the die shear tester (Dage 4000, Nordson) with 100 μm/s shear rate. The samples for cross-section inspection and porosity analysis were prepared via the methods introduced in [47–51]. The samples were first polished on a metallographic grinder and then finely polished by on an ion milling machine (Hitachi, IM4000Plus) for at least 1 h to guarantee the flatness of the surface. After taking SEM image of the cross-section, the image processing software (Image J) was adopted to screen out unwanted noises and "binarize" the SEM pictures to the threshold value in the gray scale to gain the porosity. Then, the fracture surface and the cross-section morphologies were observed by using the SEM (Zeiss GeminiSEM 300).

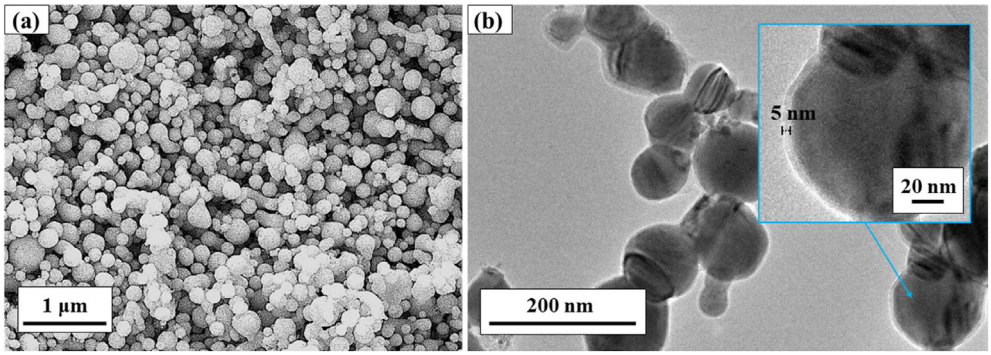

Fig. 1 – (a) SEM photo of Cu QNPs in this study. (b) TEM results of as treated Cu QNPs and the inset is the magnified TEM photo for a Cu QNP marked by a blue arrow.

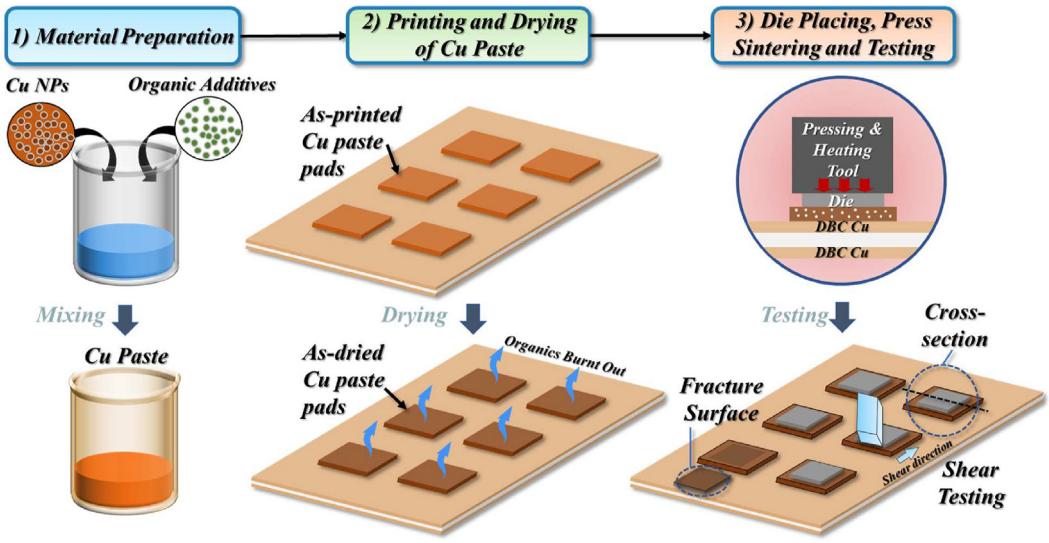

Fig. 2 – Schematic diagrams of Cu paste preparation, pressure-assisted sintering bonding process and sample testing.

Table 1 – Design of experiment for sintering process parameters study.

NO.	Pressure/MPa	Temperature/°C	Time/min
1	5	250	3
2	10	250	3
3	20	250	3
4	30	250	3
5	20	210	3
6	20	230	3
7	20	270	3
8	20	250	1
9	20	250	2
10	20	250	4

3. Results and discussion

3.1. Characteristics of Cu QNPs

Fig. 3a shows that the size of majority of the as-treated Cu is around 130–150 nm. Some particles can be found has agglomeration effect with the adjacent ones which is due to the high activity of Cu QNPs. Fig. 3b shows the XRD patterns for the original Cu QNPs, the Cu QNPs after oxidation removing treatment and the as-treated Cu QNPs stored for 30 days respectively. The as-treated Cu was stored in an open beaker in the lab. The temperature of the lab was around 25 °C. It can be seen that the main characteristic peaks at 43.29°, 50.43° and 74.13° exist for all three curves representing the lattice plane (111), (200) and (220) of pure Cu. Original Cu QNPs also possess diffraction peaks at 36.59°, 42.51° and 61.68°, corresponding to the lattice plane of (111), (200) and (220) of Cu_2O. However, for the as-treated Cu QNPs and stored as-treated Cu QNPs, there are no diffraction peaks for Cu_2O anymore, which indicates that the proposed treatment method is feasible for Cu oxidation remove and storage protection.

The Cu paste was fabricated by blending Cu QNPs with organic vehicle. The organic vehicle was comprised of solvent, resin and reductant. To determine the appropriate drying and sintering process parameter TG/DSC test was performed. Fig. 4 exhibits the TG/DSC results of the copper paste used in this work. It can be noted that, the total weight difference is around 23 wt.%, which is corresponding to the mass load of Cu metal (77 wt.%) in the paste. Moreover, from the curve the first rapid mass drop started at around 150 °C and reached an

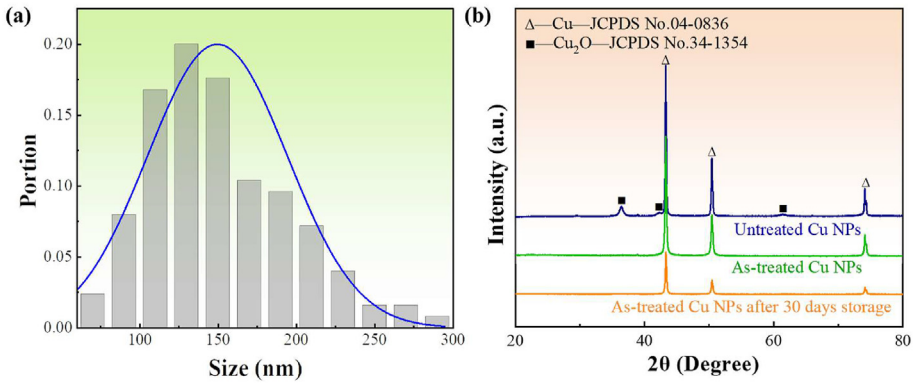

Fig. 3 – (a) Size distribution of treated Cu QNPs. (b) XRD patterns for original Cu QNPs and as-treated Cu QNPs.

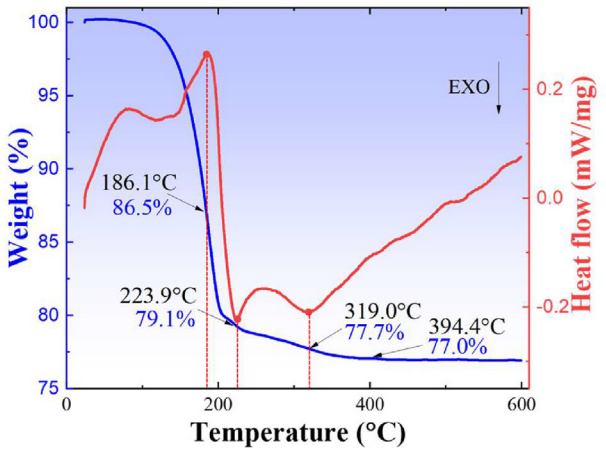

Fig. 4 – TG/DSC curve for the Cu paste in-N_2 atmosphere.

endothermal peak at 186 °C as a result of solvent evaporation. For this reason, the drying temperature was set as 150 °C. To secure the complete removing of solvent and avoid the oxidation of copper at too high temperature, the drying time was set as 5–10 min. Then the second weight loss occurred at 200 °C and reached an exothermal peak at 223.9 °C due to the burnout of organic additives. The last two slow mass drop happened at around 319 °C and 394 °C which was attributed to the burn out of residue organics.

3.2. *Effects of process parameters on the mechanical properties*

Fig. 5a and 5b and c show the results curve of shear strength versus different process parameters. From the figures, it is clear that the pressure and temperature could effectively improve shear strength, whereas the effect of time is marginal. To study the pressure effect on bonding strength first, four groups of the die attachment (DA) samples were sintered at 250 °C for 3 min with 5, 10, 20 and 30 MPa sintering pressure respectively. For each sample, five bonded dummy die were sheared off to calculate the average value and standard deviation. First, as sintering pressure increases from 5 MPa to 10 MPa, the mean shear strength is enhanced from 36.5 MPa to 61.2 MPa. The increasing rate for shear strength is 68%. Then by providing higher sintering pressure (20 MPa), the shear strength reached 100.1 MPa. The increasing rate was still high (63%). Finally, when the sintering pressure increased to 30 MPa, the shear strength increases slightly to 116.7 MPa, with only 17% increasing rate compared with 20 MPa-pressure sintering. The microstructural reason for the positive effect of applied pressure on shear strength improvement will be discussed in the following sections.

Fig. 5b reveals the temperature effect on the shear strength of sintered Cu joint. It shows similar trend as pressure effect. The applied pressure was set as 20 MPa and sintering time was kept as 3 min. When the sample was sintered only with 210 °C, it shows less than 30 MPa mean shear strength, which is insufficient for electronics packaging [19]. Surprisingly, when only added up 20 °C sintering temperature, it provided over 70 MPa shear strength with 135% increasing rate. In addition, shear strength over 100 MPa was obtained at above 250 °C sintering temperature. Combining the DSC and shear test results, it denotes that only temperature over 230 °C can ensure the organic compounds decomposition and sintering process completion, which was also proved in previous studies [41]. It is worth noting that for higher temperature such as 270 °C, the standard deviation of shear strength is also huge. One reason could be that high temperature caused warpage of substrate and then influence the effective contact area and applied pressure to different dummy die. The other reason is that higher temperature may increase the risk of copper oxidation during sintering, since high oxygen element content is found from EDS results of next section. From results discussed above, it is found that with the increase of sintering temperature, the shear strength exhibits noticeable increase.

Fig. 5c displays the relationship between sintering time and shear strength. From the perspectives of industrial manufacturing, the unit per hour (UPH) of yielding is critical. Normally, each batch of sintering process for electronics packaging needs to be less than 5 min. Therefore, in this work dwell time scope less than 4 min was selected. The sintering temperature was set as 250 °C and applied pressure was 20 MPa. It can be easily found from the figure that even in short sintering time, the material can still obtain over 100 MPa shear strength. There is no statistical difference among samples sintered for 1 min to 4 min. For one thing, this result implies that the material in this work is suitable for the fast sintering for the industrial application. For another thing, although longer sintering time can secure more complete sintering structure, 100 MPa bonding strength is already high enough for packaging application. Thus, longer time case will

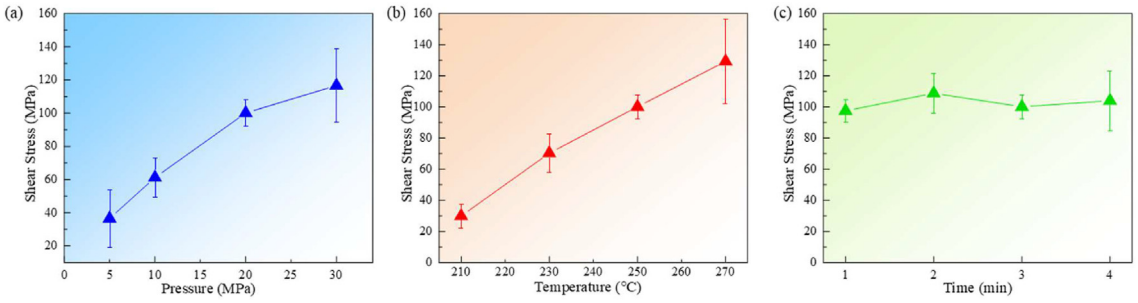

Fig. 5 – Shear stress results versus different (a) sintering pressure (5, 10, 20 and 30 MPa), (b) sintering temperature (210, 230, 250 and 270 °C), (c) sintering time (1, 2, 3 and 4 min) for copper sintered joint samples.

not be discussed in this work. In summary, 250 °C, 20 MPa and 3 min are the optimized process parameters for the nano copper paste in this study, considering mechanical strength, UPH and results stability. Table 2 shows the typically reported die shear strength of both Ag sintered joints [47] and Cu sintered joints [32,52,53]. The shear strength obtained in the present study is higher than not only the commercial Ag sintering material, but also the typical current Cu sintering paste. Furthermore, compared with nano Ag sintering with precious metal and nano Cu sintering with smaller particles, the QNPs Cu paste has advantages such as higher UPH and lower cost.

3.3. *Fracture modes*

In order to determine the effect of sintering conditions on the fracture mode, the fracture surface morphologies for sheared off samples were observed by SEM. First for samples sintered with different sintering pressure, the global views of sheared off samples are shown in Fig. 6a to d. It is identified that each sample contains both a smoother, low-contrast region and a rougher, high-contrast region. EDS results for position A and B in Fig. 6b verified that high-contrast region and low-contrast region are mainly Cu (94.81 wt%) and Ag (99.31 wt.%) individually. Therefore, the smoother region is the exposed Ag metallization layer on the dummy die and the rougher one is the residue copper sintered layer.

Fig. 6e–6h are the 2000 × magnified photos of the sintered Cu residual regions as marked by blue frame in Fig. 6a to d. It shows clear relationship between the fracture surface morphology and the sintering pressure. In Fig. 6a, along the fracture direction, it contains relative flat broken facet on certain QNPs, as marked by red arrows. Such fracture morphology indicates the brittle fracture process. Moreover, the magnified photos also reflect the relationship between microstructural evolution and shear strength during the sintering. Neck growth between adjacent Cu QNPs can be clearly observed as marked by green arrows. Apparently, the sintering is incomplete since the necking width is short and all QNPs still remain spheroidal shape. Besides the neck structure, large-size connected pores also exist in between. In this case, the primary adhesion forces in the joint were van der Waals forces from particle adsorption [54]. These structures can be the reason for the relatively low shear strength of this sample. By contrast, some plastic deformation positions exist in the fracture facets (marked by red arrows in Fig. 6f) of 10 MPa

Table 2 – Typical die shear stress in this study and other studies.

Material	Sintering temperature	Sintering pressure	Sintering time	Shear strength	Reference
Commercial sinter Ag	250 °C	30 MPa	3 min	73.4 MPa	H. Zhang et al. [47]
Cu	275 °C	2 MPa	10 min	35.1 MPa	Y. Mou et al. [52]
Cu	225 °C	20 MPa	5 min	63 MPa	W. Choi et al. [32]
Cu	280 °C	9 MPa	5 min	> 80 MPa	J. Jo et al. [53]
Cu	250 °C	20 MPa	3 min	100.1 MPa	This work

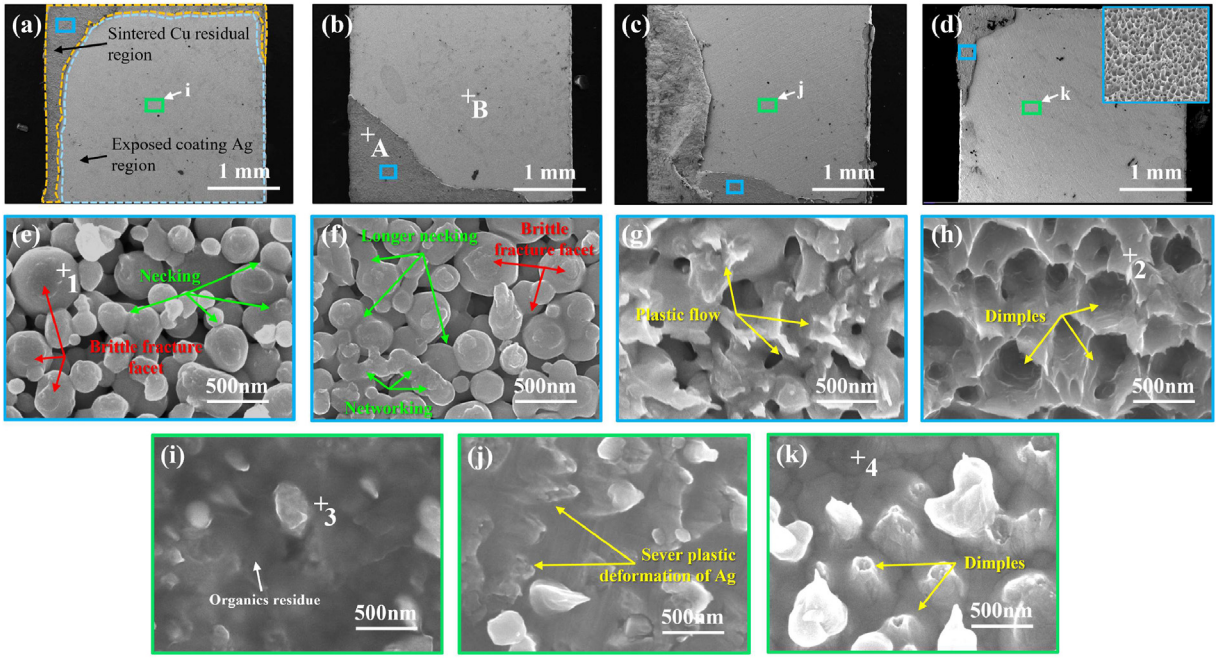

Fig. 6 – SEM fracture morphology of sheared-off dice and partial magnified images for blue and green frame regions. This group of samples were sintered at 250 °C for 3 min with different pressure: (a) (e) and (i) 5 MPa; (b) and (f) 10 MPa; (c), (g) and (j) 20 MPa, (d), (h) and (k) 30 MPa.

sample. Apart from that, there is not only longer neck size compared with that of 5 MPa sample, but also the increased number of necking regions for each QNPs, as marked by green arrows as well. This can be the microstructural reason of strength improvement for this sample.

Based on above mentioned observations, it is deduced that the 5 MPa and 10 MPa sintered samples have the mixed (more adhesive) fracture mode as shown in Fig. 7a. In addition, Fig. 6g and h indicate that the 20 MPa and 30 MPa samples have severe plastic deformation on the fracture regions. More significantly, the sintered Cu layer of 30 MPa sample left on the dummy dice exhibited the severest plastic deformation and contained a uniform distribution of dimple structure as yellow arrows marked. In addition, Cu QNPs in Fig. 6g and h have already formed large area of network with wide necking size, which indicates that the sintering process for 20 MPa and 30 MPa sample are at near complete stage. Also, the pores in between became smaller and were isolated by the Cu network. These results are corresponded to the excellent mechanical strength for them, and meanwhile representing the mixed (more cohesive) fracture mode as shown in Fig. 7b. Among these samples, the crack first initiated from one side (bottom surface of dummy dice or top surface of DBC), and then propagate into the copper joint layer. At certain point, the crack finally transferred into the opposite side.

Moreover, Fig. 6i, j and k are the 2000 × magnified photo of the exposed coating Ag region marked by green frame in Fig. 6a, c and d. Fig. 6i shows that there were small isolated particles found embedded in the translucent background substance. EDS result (as shown in Fig. 8a) at position 1 and 3 show that the particles were mainly Cu QNPs, and the translucent substance was mainly carbon residues tiled on the coating Ag layer. Based on the DSC/TG result, expect for solvent, the organic additives and coating agent material on Cu QNPs would start to be burnt out at temperature above 223.9 °C. Therefore, during the sintering process of this group (250 °C, 3 min with different pressure), the organics was indeed evaporated. Normally, with the help of pressure the gas would be expelled quickly [55]. However, for low pressure (5 MPa, Fig. 6e and i) scenario, the outgassing process is slow and incomplete within 3 min. Therefore, large amounts of organics did not have time to expel out and was gathered and locked insides the sintered layer. In contrast, for higher pressure scenario (30 MPa, Fig. 6j, k) the carbon content was dramatically reduced. Apart from that, in Fig. 6j and k more deformed and broken sintered Cu structure was found on the coating Ag. Also, with the increase of sintering pressure there are more and more Ag element left on copper sintered layer region and Cu element on exposed metallization layer region respectively (position 2 and 4). The above-mentioned results indicate that higher pressure may promote the atomic diffusion during the sintering process, and at the same time, effectively enhance bonding strength by promoting the necking growth, networking formation, pores isolation and brittle-ductile fracture transformation.

The fracture morphology SEM photos of sample sintered at 210 °C–270 °C are shown in Fig. 9. Combined with the discussion in the previous part it is proved that the exposed layer of 210 °C sample was sintered Cu. Thus, the sample sintered at 210 °C shows adhesive fracture mode as shown in Fig. 7c. Unlike other samples, the fracture area for 210 °C sintered sample is mainly on the interface between substrate and sintered layer. It suggests that the Cu sintered layer did not form strong bonding with DBC substrate yet. Although some particles were found to be slightly deformed, most of Cu QNPs kept their sphere-like shape and yielded short necking structure (marked with green arrows) with its adjacent particles, which again represented that such at such low temperature, sintering was at incomplete stage. Additionally, huge pores distributed randomly around particles and therefore created

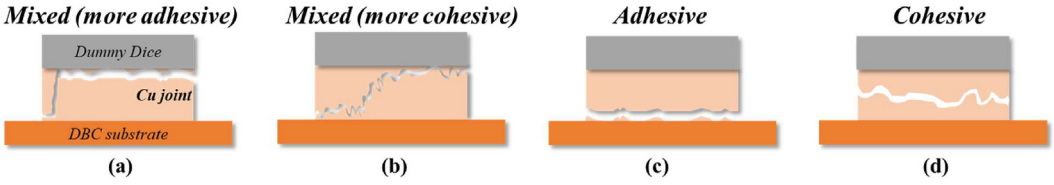

Fig. 7 – Schematic diagrams of shear test fracture mode. (a) mixed mode with more adhesive portion, (b) mixed mode with more cohesive portion, (c) pure adhesive mode, (d) pure cohesive mode.

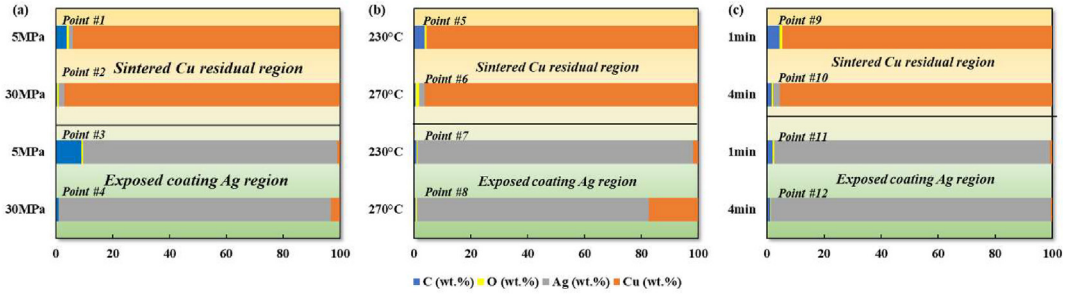

Fig. 8 – EDS results for the marked positions in the SEM fracture morphology figures. (a) points in Fig. 6; (b) points in Fig. 9; (c) points in Fig. 10.

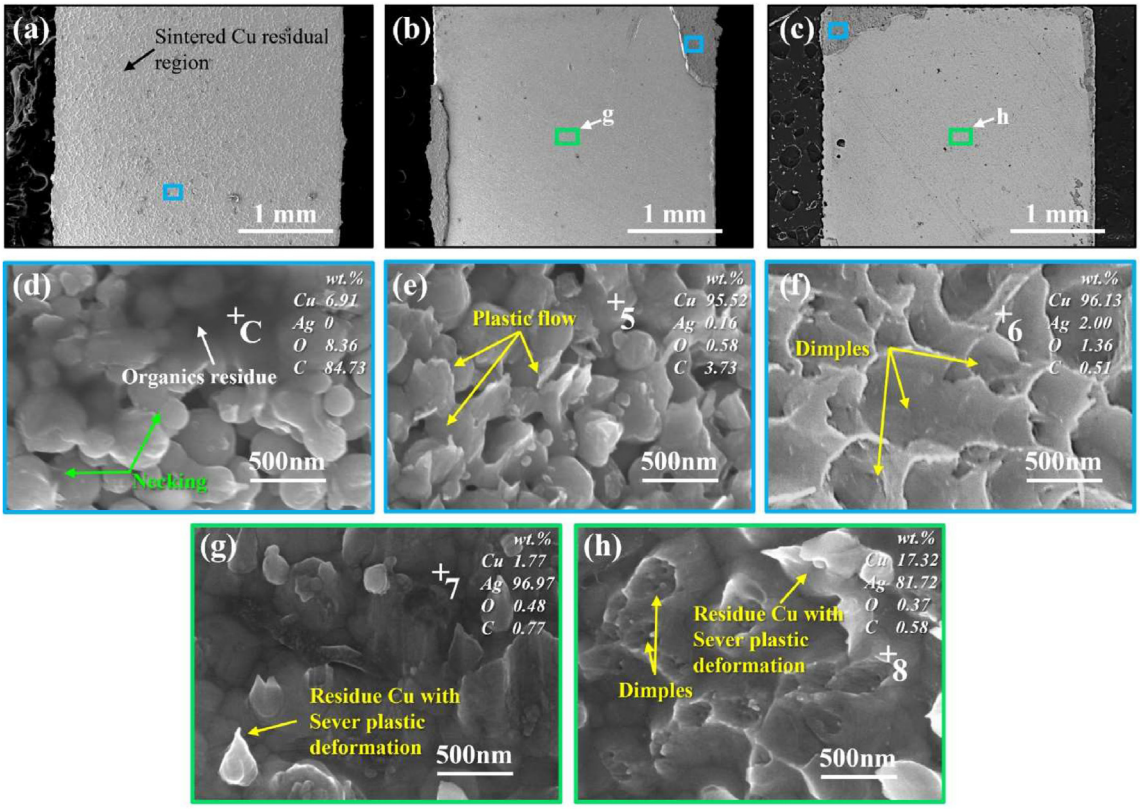

Fig. 9 – SEM fracture morphology of sheared-off dice and partial magnified images for blue and green frame regions. This group of samples were sintered with 20 MPa for 3 min at different temperatures: (a) and (d) 210 °C; (b) (e) and (g) 230 °C; (c), (f) and (h) 270 °C.

relatively loose structure. Fig. 9e shows the magnified image of blue frame area in Fig. 9a. The large amount of dark translucent substance was also found in this region. The EDS result at position C proves that it is organics residues laying around sintered Cu, containing large amount of carbon and oxygen. This can be attributed to that sintering temperature was lower than the organics evaporating temperature. In addition, it can be found that the surface of organic residue is smooth, and thus, there was neither physical nor chemical bonding between the organic gathering residue and the substrate surface. Since on the interface some regions were occupied by such substance, it reduced the region for bonding between Cu sintered layer and substrate surface. Consequently, it further reduced the bonding strength of this sample.

Fig. 9b, c, e and f indicate that both samples sintered at 230 °C as well as 270 °C are mixed mode (with more cohesive portion) For 230 °C–270 °C samples fracture occurs on the interface but propagated into the sintered layer. Most of sintered layer were left on the substrate whereas only slight amount remained on the dummy die. Therefore, the bonding between sintered layer and the substrate is relatively high. The magnified view of 230 °C sample fracture surface shows relatively denser microstructure with obvious mono-directional plastic flow as marked by yellow arrows. Hence, before the fracture, moderate plastic deformation occurred at these areas. Similarly, the magnified view of 270 °C sample shows sintered Cu structure with large deformation and uniformly distributed dimple structures on both the exposed Ag metallization layer and the residue copper sintered layer. Such deep dimples indicate even more sever plastic deformation during the shear test [45]. Furthermore, the EDS results for position 5 to 8 reveals that higher temperature effectively increased the Cu and Ag interdiffusion, and at the same time helped to remove organic residues more completely.

Fig. 10 shows the fracture morphology SEM photos of sample sintered for 1, 2 and 4 min. We found that the fracture modes for this sample group all belong to mixed mode (more cohesive portion). In such fracture mode, crack initiated from one interface and propagated into sintering layer and then fast transferred onto the other interface on opposite side. Similarly, EDS results in Fig. 8c of position 9 to 12 prove that few of sintering material was taken away by dummy die but most of the Cu sintered material was remained on the substrate. Fig. 10d–10f are the magnified view of the position marked by blue frame in Fig. 10a to c. From these figures, all the sintering material has huge necking formed and no spheroidal shape existed anymore. Distinct plastic flow can be found in all samples and obvious dimple microstructure exists in the 4 min sintering one, which is corresponding to the high shear strength for all samples. By further comparing the EDS results for samples sintered for different dwell time, it is found that the Cu content and Ag content are almost unchanged on the copper sintered residue (CSR) layer and the exposed silver metallization (ESM) layer on the dummy die.

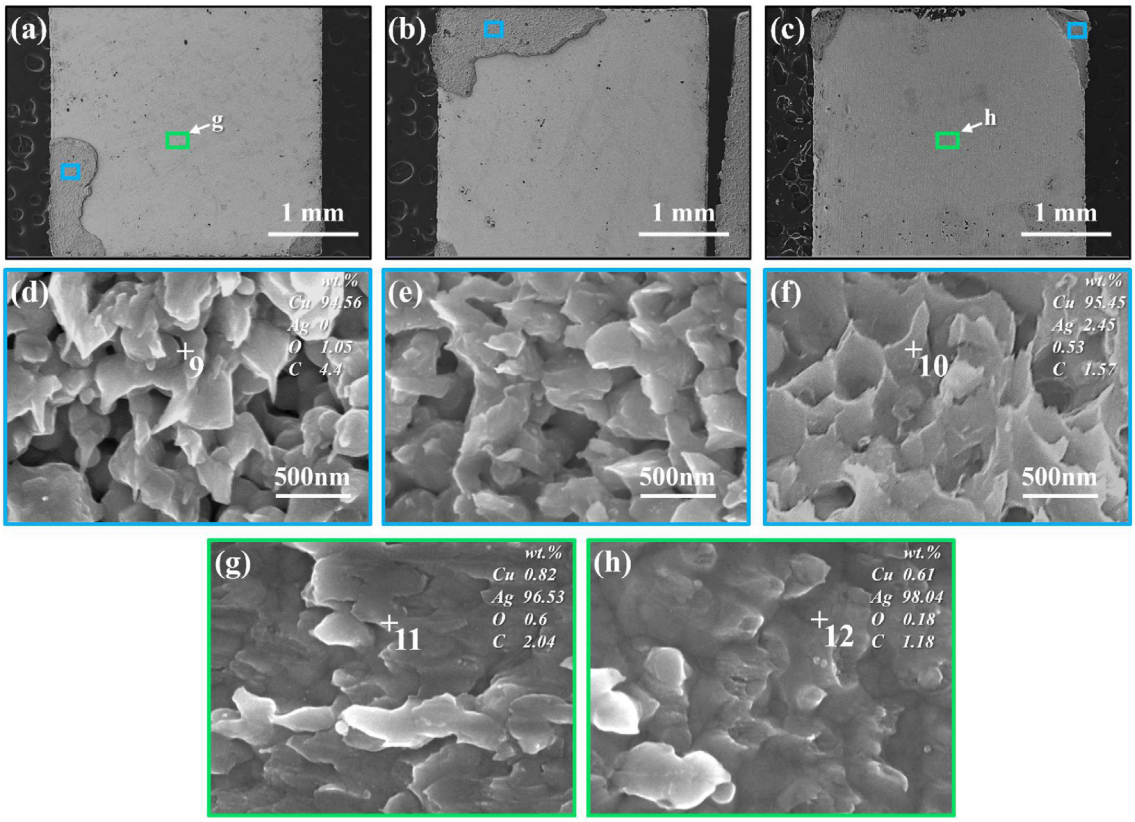

Fig. 10 – SEM fracture morphology of sheared-off dice and partial magnified images for blue and green frame regions. This group of samples were sintered at 250 °C with 20 MPa for different dwell time: (a) (d) and (g) 1 min; (b) and (e) 2 min; (c), (f) and (h) 4 min.

Therefore, it is deduced that within 1–4 min, there is little difference on atomic diffusion process in the Cu sintered body and bonding interface.

3.4. *Interface evolution*

Next, the cross-section microstructure inspection was conducted for each sintered bonding sample in order to study the densification effect and interface diffusion of sintered layer. From Fig. 11 it can be seen that the sintering pressure has marked impact on the morphology of both the Cu sintered layer and the bonding interface. Fig. 11 a to d and Fig. 11 e to h display morphologies near the bonding interface between sintered layer and Ag metallization layer of dummy die as well as morphologies near the bonding interface between sintered layer and substrate, respectively.

To begin with, it can be clearly observed that with the increase of sintered pressure, 1) the number and size of interface voids on the Ag–Cu interface decreased dramatically first from 5 MPa to 20 MPa, and then increased a little with 30 MPa. 2) the voids on the substrate Cu–Cu layer interface decreased over time. As discussed in previous section, for 5 MPa sample, the sintering was not done thoroughly, causing short neck growth between Cu QNPs.

In addition, the removing of organics was incomplete. Lots of transparent substance which was proved to be the organic residue was found on each interface hindering the contact between Cu sintered layer and the surface to be attached. Plenty of large-size voids connected with each other and formed the large-size cracks as marked by red dotted box. With the increase of sintering pressure (10 MPa, 20 MPa and 30 MPa), the size of sintered neck and network of sintered body increased. Also, the organics residue is hardly to be found on the interface anymore. More Cu QNPs was able to be connected with the upper and lower surface. For 20 MPa and 30 MPa sample, the voids on the Cu–Cu interface were diminished by further increasing pressure forming a voids-free complete bonding region. This is believed as one of the most important reasons for bonding strength improvement and fracture mode transition found in the previous section. However, at the upper interface, the voids size was increased again. This was reported in other studies as well. This is mainly attributed to the unequal Ag to Cu and Cu to Ag interdiffusion speed at this region. More Ag atoms were transported into Cu and left the so-called Kirkendall voids [45,56]. Fig. 11i–11l are the magnified photos for the sintered layer. Necking and networking morphologies can be clearly observed. Previous research [48,49,57] found that intrinsic pores existed in the sintering joints and affected the bulk mechanical properties such as elastic modulus, yield strength, ultimate tensile strength and so on. Thus, analyzing porosity property of sintered structure is significant. By applying Image J analysis, the porosity value for each sample can be extracted. With low sintering pressure (5 MPa) it shows large sized pores with the highest porosity (26.5%). Via

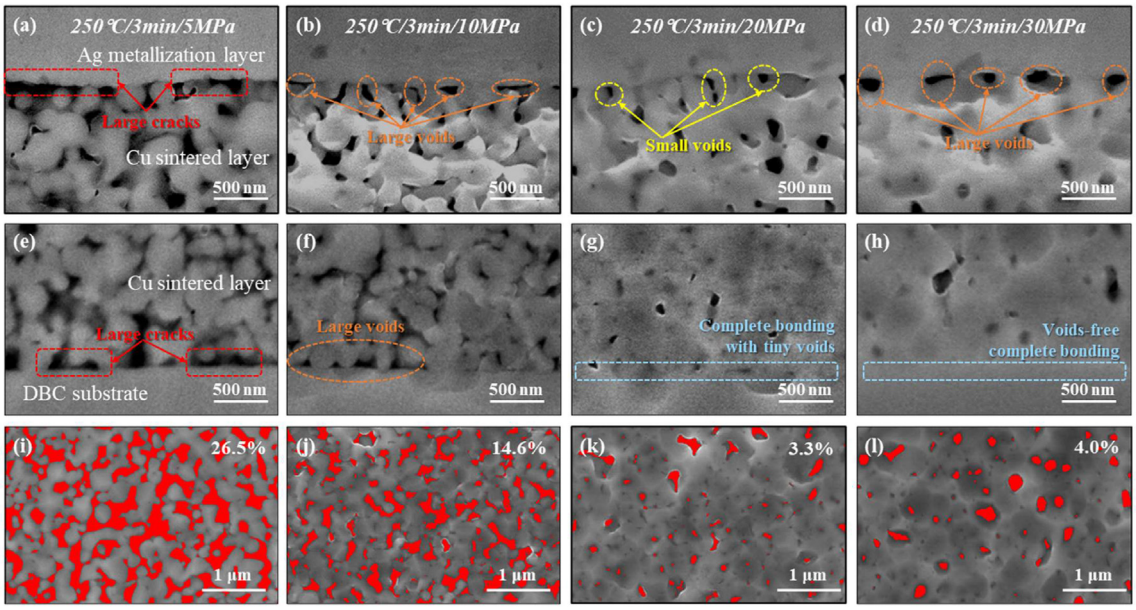

Fig. 11 – SEM images of cross-section morphology with different sintering pressure: (a)–(d) near the Cu–Ag bonding interface; (e)–(h) near the Cu–Cu bonding interface; (i)–(l) sintered body.

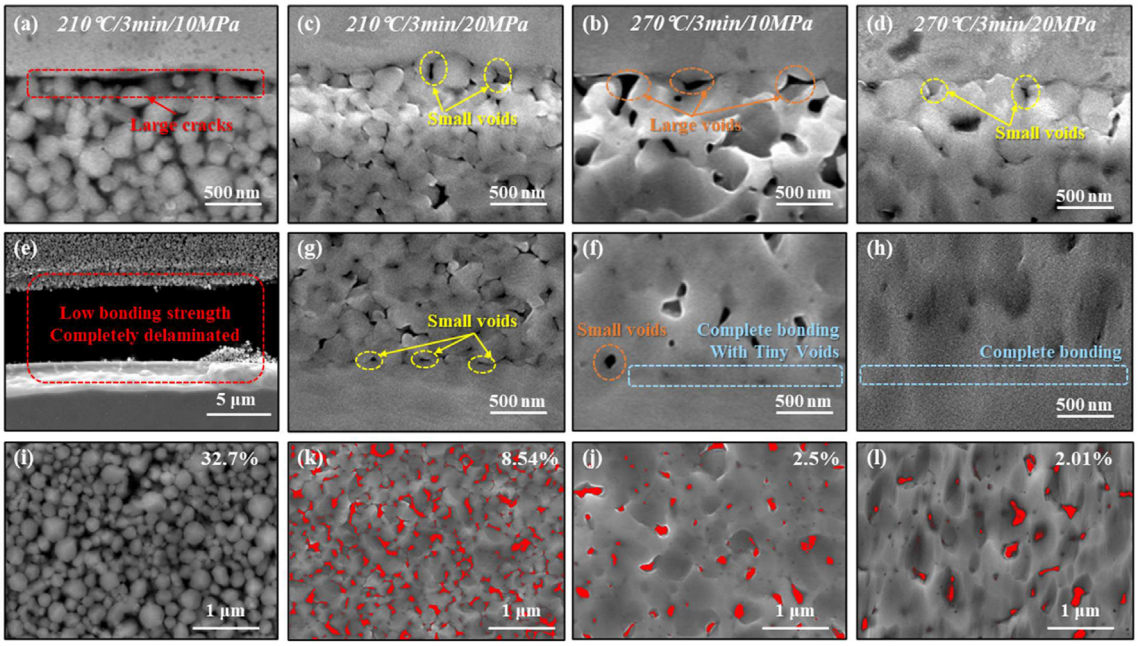

Fig. 12 – SEM images of cross-section morphology with different sintering pressure and at different sintering temperature: (a)–(d) near the Cu–Ag bonding interface; (e)–(h) near the Cu–Cu bonding interface; (i)–(l) sintered body.

increasing sintering pressure to 10 MPa and 20 MPa, the pore size decreased dramatically to 14.6% and 3.3%. However, by further increasing bonding pressure to 30 MPa, the porosity reversely increased to 4.0%. The reason for the porosity increase is the sintered body shrinkage at the final sintering stage. Higher pressure can provide more energy for NPs coalescence, which can promote sintering process and cause the shrinkage of sintered body [58].

To further study the cooperative effect of pressure and temperature on the microstructure, the SEM cross-section figures for samples sintered at 210 °C with 10 MPa and 20 MPa, and at 270 °C with 10 MPa and 20 MPa were analyzed (see Fig. 12). For low temperature scenario (210 °C), when pressure is 10 MPa, Cu QNPs were only pushed to contact with each other and slightly sintered to form short necks. Due to the incomplete burnt out of organic additives, lots of residues were left inside the sintering body and on the bonding interface. Similar to low pressure case in previous discussion, large cracks were formed on the interface and therefore causing the delamination after sintering. By increasing pressure to 20

MPa, the QNPs was pushed together closer, and the necks length grew effectively. It also can be deduced that the pressure can affect isolation of pores more than temperature does. The porosity reduced from 32.7% to 8.54%. Most of pores were already isolated. The rest pores only have less than 0.5 um diameter distributed in the sintered network. On both the upper and lower interface, the QNPs was connected with the surface by diffusion, providing over 30 MPa bonding strength. At high temperature, the Cu particles have almost completely sintered forming strong networking. The sintering body of both 10 MPa and 20 MPa cases show high density. The difference comes from the pores size and amounts. With increasing of pressure, the voids became smaller, and on the Cu–Cu interface, most of voids were diminished leaving a complete bonding region. Compared with low temperature scenario, the porosity also shows slightly decrease from 8.54% to 7.83% for 210 °C and 230 °C and then from 3.30% to 2.01% for 250 °C and 270 °C.

Next, the comprehensive effect of pressure and dwell time on the microstructure was investigated. From cross-section photo in Fig. 13, the effect of pressure on the microstructure for of different dwell time cases is clear. With the increase of sintering pressure for both 1 min and 4 min cases, 1) again the sintering density increased effectively. 2) the number and size of interface voids on both of the Ag–Cu and Cu–Cu interface decreased dramatically, 3) and uniform bonding interface were formed. Then, by further comparing the results for samples with same sintering temperature and pressure but different time, it can be found that there is little difference on the microstructure. Combined with shear stress results in Fig. 5c, it shows that, the sample can already be well sintered at 250 °C with 20 MPa within 1 min. However, longer sintering time is necessary to ensure the formation of rigid sintering body networking as shown in Fig. 13b and d.

3.5. *Bonding mechanism*

During the pressure assisted sintering, with the help of temperature, dwell time and pressure, the residue polymer content will be burnt out and degassing from sintered body. At the same time, the copper QNPs contact with their adjacent particles and substate surface, forming mechanical-chemical bonding, providing high bonding strength. In low temperature case, the shear strength was relatively low, and the fracture surface was adhesive mode. Microstructural schematic drawing in Fig. 14 shows that the necks between Cu particles were short. The EDS and DSC/TG results prove that the organics in the paste was not completely removed. Therefore, the organics residues were distributed in the sintering body and tiled on the Ag–Cu interface. Therefore, the weak bonding in this case is due to the comprehensive effect of insufficient sintering energy provided by low temperature and organics hindrance on the particle contact. By increasing the pressure at low temperature, although the sintering was still incomplete, the contact area of each particle and the density of sintered body and was enhanced. Additionally, the organics was squeezed out and thus providing more space for particle coalescence.

When sintering at low pressure, it shows low shear strength and mixed mode but with more adhesive portion. Fig. 14 indicates that fragile bonding is due to incomplete neck growth and large amounts of pores in between. Meanwhile, although organics was evaporated at 250 °C, without high pressure it could not be expelled quickly. Thus, most of organics again condensed on the upper surface, leaving large area of unconnected delamination on the Ag–Cu interface as observed by SEM and EDS. By increasing temperature at low pressure, the bonding strength and microstructure was improved. It is found that higher sintering temperature

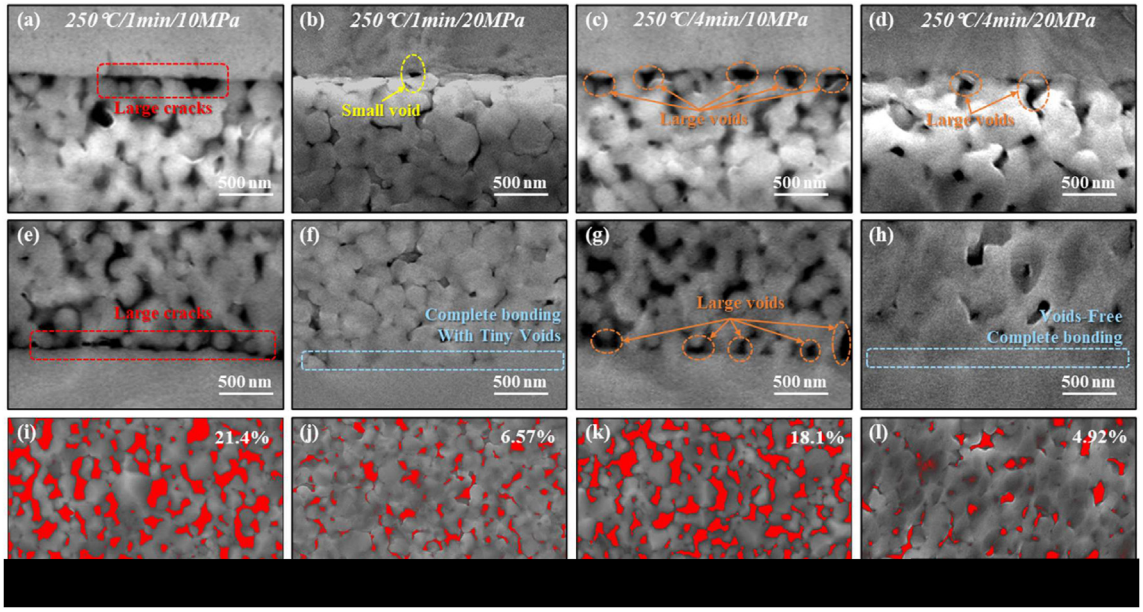

Fig. 13 – SEM images of cross-section morphology with different sintering pressure and for different time: (a)–(d) near the Cu–Ag bonding interface; (e)–(h) near the Cu–Cu bonding interface; (i)–(l) sintered body.

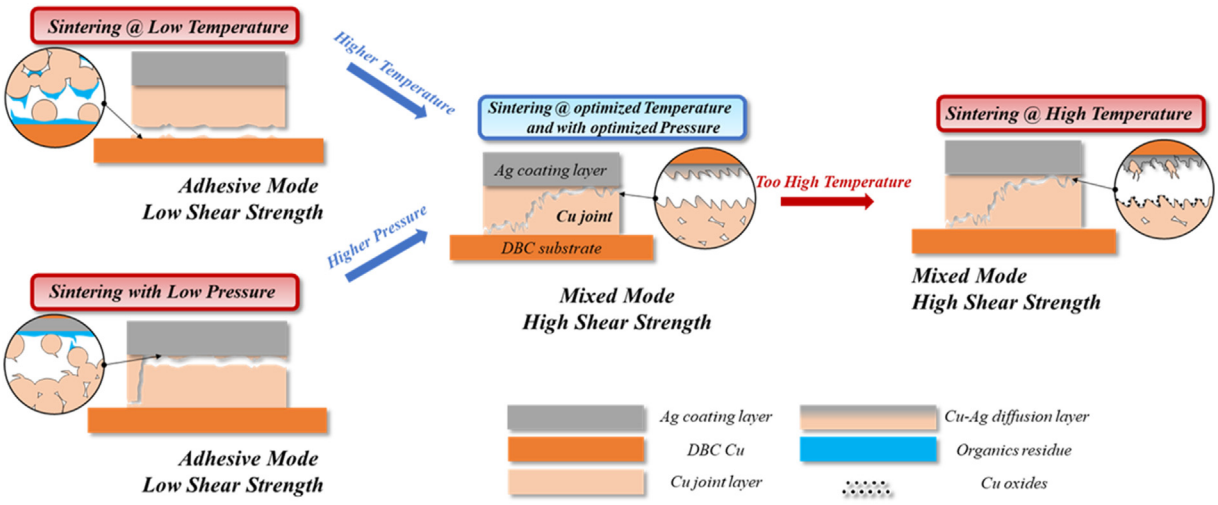

Fig. 14 – Schematic diagram of sintering mechanism for different process conditions.

increased Cu content in both of the Cu sintered joint and the Ag coating layer on the dummy die, and as a result, forming the Cu–Ag metallization bonding. Hence, the higher temperature effectively improved the atomic diffusion in the bonding process. Meanwhile, the content of carbon decreased with increase of sintering temperature, which is because polymer will burn out more thoroughly at higher temperature.

However, when the temperature was too high, there was oxidation issue. In the SEM fracture morphology photo we found that there was small hillocks and corresponding small pits on the dimples with couple of nanometers in high temperature case. Combined with EDS results, it is found that the oxygen content was higher than other samples. Such hillocks were also observed in some studies [6] which was believed to be copper oxides generated during material treatment or high-temperature sintering. Other studies also reported [59] that the copper oxide formed during reliability test may enhance the bonding strength. It is deduced that the small hillocks could improve the bonding strength by mechanical interlocking effect in this study. However, the microstructural evolution and negative effect during reliability test of such structure is still unclear. Moreover, the interface on Cu sintering layer and Ag coating layer on the chip was observed to contain more voids than that of the interface between Cu sintering layer and Cu ceramic substrate. This is mainly due to the unequal diffusion rate of Ag to Cu and Cu to Cu. Consequently, most of fracture surface appeared at the Ag–Cu interface side.

3.6. *Feasibility study of copper sintering for SiC MOSFET die attachment application*

To verify the feasibility of the nano copper as the DA material for WBG power electronics devices, a 1200 V/200 A SiC MOSFET DA sample on bare copper AMB substrate was fabricated as shown in Fig. 15a. This sample was sintered at 250 °C with 20 MPa for 3 min and the gate and source of the chip were interconnected onto the substrate by using 5 mil and 12 mil Al bonding wires, respectively. The static output I–V characteristics (V_{GS} = 15 V) of the sample was obtained by using Agilent B1505A power device analyzer at both room temperature and 150 °C as seen in Fig. 15b and c. At room temperature, R_{dson} is measure as 10.52 mΩ for the DA sample. When increase the temperature to 150 °C the curve shifts to the right and the measured R_{dson} increased to 11.91 mΩ as well. However, theses test results are still within the scope of the theoretical calculation result of the parallel structure of two bare chips (8.5–12 mΩ, calculated with the data in the datasheet). The measured static characteristics proves that the copper sintering technique in this work is feasible for WBG power electronics packaging process.

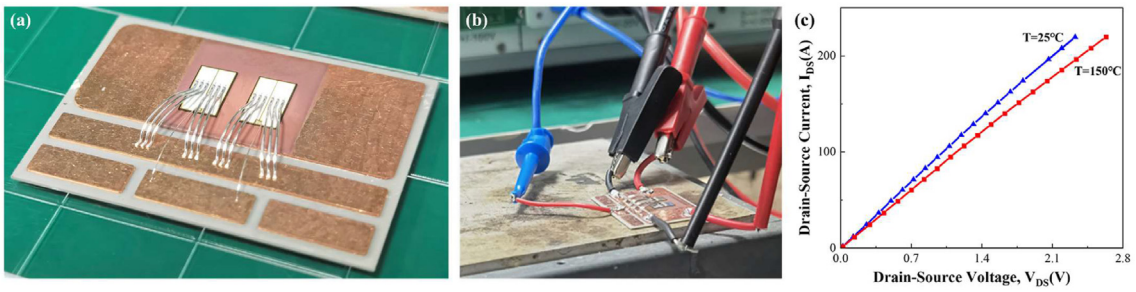

Fig. 15 – (a) Image of 1200 V/200 A SiC MOSFET DA sample. (b) Image of static testing of the sample on a heating plate. (c) The static output characteristics of the sample.

4. Conclusion

In this work, a die attachment process SiC electronics packaging. was demonstrated by applying pressure-assisted sintering process. First of all, Cu QNPs reductive pretreatment was conducted to the commercial Cu particles. It is proved that the copper oxidation was effectively removed and the Cu QNPs were protected by the reductant for long time. Then the nano copper paste was fabricated by using as-treated Cu QNPs blended with organic vehicles. Robust bonding of Cu sintering on bare copper DBC substrate was achieved. The effect of temperature, pressure and time on the sintering bonding strength and microstructural evolution was deeply studied. 36.5 MPa shear strength was achieved when applied 5 MPa low pressure. By increasing pressure to 30 MPa, it shows the best die shear strength of 116 MPa, accomplished with a sintering temperature of 250 °C for 3 min. Temperature also plays an important role for bonding strength improvement by promoting NPs coalescence and atomic interdiffusion on the interface. Temperature between 210 °C and 230 °C could provide strength over 30 MPa. Such low strength is due to both of the incomplete burnt out of organics and Cu QNPs sintering. When increased to 270 °C, the shear strength was extremely enhanced to over 120 MPa. In addition, it turns out that high bonding is account for the positive effect of pressure and temperature on promoting the necking growth, sintering networking formation, pores isolation and brittle-ductile fracture transformation. Moreover, in the present short-time range, time will insignificantly affect the microstructure and bonding strength. Finally, the optimized sintering process parameters (250 °C with 20 MPa for 3 min) for the industrial application was proposed. A 1200 V/200 A SiC MOSFET DA sample on bare copper AMB substrate was fabricated by using the present sintering copper material. Both of the room-temperature and high-temperature performance are satisfying, which indicates that the present material is feasible for WBG power electronics packaging process.

Declaration of Competing Interest

The authors declare that they have no known competing financial interests or personal relationships that could have appeared to influence the work reported in this paper.

Acknowledgement

This work was supported by the National Key R&D Program of China (2018YFE0204600), the Shenzhen Fundamental Research Program (JCYJ20200109140822796), and the NSQKJJ under grant K21799119.

Appendix A. Supplementary data

Supplementary data to this article can be found online at https://doi.org/10.1016/j.jmrt.2022.05.122.

REFERENCES

[1] Mai T-D, Van den Broeck G, Pevere A, Driesen J. Power electronics for potential distribution DC power evolution: a review. In: 2016 IEEE international energy conference (ENERGYCON); 2016. p. 1–6. https://doi.org/10.1109/ENERGYCON.2016.7513923.

[2] Rahrovi B, Ehsani M. A review of the more electric aircraft power electronics. In: 2019 IEEE Texas power and energy conference (TPEC); 2019. p. 1–6. https://doi.org/10.1109/TPEC.2019.8662158.

[3] Chen C, Suganuma K. Microstructure and mechanical properties of sintered Ag particles with flake and spherical shape from nano to micro size. Mater Des 2019;162:311–21. https://doi.org/10.1016/j.matdes.2018.11.062.

[4] Noh S, Choe C, Chen C, Suganuma K. Heat-resistant die-attach with cold-rolled Ag sheet. Appl Phys Express 2018;11:016501. https://doi.org/10.7567/APEX.11.016501.

[5] Suganuma K, Nagao S, Sugahara T, Yokoi E, Zhang H, Jiu J. Silver sinter joining and stress migration bonding for WBG die-attach. In: 2016 international symposium on 3D power electronics integration and manufacturing (3D-PEIM); 2016. p. 1–17. https://doi.org/10.1109/3DPEIM.2016.7570554.

[6] Liu X, Nishikawa H. Improved joint strength with sintering bonding using microscale Cu particles by an oxidation-reduction process. In: 2016 IEEE 66th electronic components and technology conference (ECTC); 2016. p. 455–60. https://doi.org/10.1109/ECTC.2016.248.

[7] Li D, Mei Y, Xin Y, Li Z, Chu PK, Ma C, et al. Reducing migration of sintered Ag for power devices operating at high temperature. IEEE Trans Power Electron 2020;35:12646–50. https://doi.org/10.1109/TPEL.2020.2994343.

[8] Lu G-Q, Mei Y, Wang M, Li X. Low-temperature silver sintering for bonding 3D power modules. In: 2019 6th international workshop on low temperature bonding for 3D integration (LTB-3D); 2019. https://doi.org/10.23919/LTB-3D.2019.8735123. 19–19.

[9] Xie Y, Wang Y, Mei Y, Xie H, Zhang K, Feng S, et al. Rapid sintering of nano-Ag paste at low current to bond large area (>100 mm^2) power chips for electronics packaging. J Mater Process Technol 2018;255:644–9. https://doi.org/10.1016/j.jmatprotec.2018.01.017.

[10] Yan H, Mei Y-H, Wang M, Li X, Lu G-Q. Pressureless sintering multi-scale Ag paste by a commercial vacuum reflowing furnace for massive production of power modules. J Mater Sci Mater Electron 2019;30:9634–41. https://doi.org/10.1007/s10854-019-01297-x.

[11] George E, Das D, Osterman M, Pecht M. Thermal cycling reliability of lead-free solders (SAC305 and Sn3.5Ag) for high-temperature applications. IEEE Trans Device Mater Reliab 2011;11:328–38. https://doi.org/10.1109/TDMR.2011.2134100.

[12] George E, Pecht M. Process occurs through atomic transportation (mass transportation) at the contact area of particles. Microelectron Reliab 2016;65:1–7. https://doi.org/10.1016/j.microrel.2016.07.150.

[13] Quintero PO, McCluskey FP. Temperature cycling reliability of high-temperature lead-free die-attach technologies. IEEE Trans Device Mater Reliab 2011;11:531–9. https://doi.org/10.1109/TDMR.2011.2140114.

[14] Gao Y, Chen C, Nagao S, Suganuma K, Bahman AS, Iannuzzo F. Highly reliable package using Cu particles sinter paste for next generation power devices. In: PCIM europe 2019; international exhibition and conference for power electronics, intelligent motion. Renewable Energy and Energy Management; 2019. p. 1–4.

[15] Yuan Y, Wu H, Li J, Zhu P, Sun R. Cu-Cu joint formation by low-temperature sintering of self-reducible Cu nanoparticle

paste under ambient condition. Appl Surf Sci 2021;570:151220. https://doi.org/10.1016/j.apsusc.2021.151220.
[16] Zhang B, Damian A, Zijl J, van Zeijl H, Zhang Y, Fan J, et al. In-air sintering of copper nanoparticle paste with pressure-assistance for die attachment in high power electronics. J Mater Sci Mater Electron 2021;32:4544–55. https://doi.org/10.1007/s10854-020-05196-4.
[17] Zhang Y, Zhu P, Li G, Chen L, Cui C, Zhang K, et al. Easy separation of cuo nanocrystals with high catalytic activity. Mater Lett 2018;212:332–5. https://doi.org/10.1016/j.matlet.2017.10.127.
[18] Chen C, Iwaki A, Suetake A, Sugiura K, Kanie K, Suganuma K. Low temperature Cu sinter joining on different metallization substrates and its reliability evaluation with a high current density. In: 2021 33rd international symposium on power semiconductor devices and ICs (ISPSD); 2021. p. 387–90. https://doi.org/10.23919/ISPSD50666.2021.9452283.
[19] Chen TF, Siow KS. Comparing the mechanical and thermal-electrical properties of sintered copper (Cu) and sintered silver (Ag) joints. J Alloys Compd 2021;866:158783. https://doi.org/10.1016/j.jallcom.2021.158783.
[20] Bhogaraju SK, Mokhtari O, Conti F, Elger G. Die-attach bonding for high temperature applications using thermal decomposition of copper(ii) formate with polyethylene glycol. Scripta Mater 2020;182:74–80. https://doi.org/10.1016/j.scriptamat.2020.02.045.
[21] Gao Y, Zhang H, Li W, Jiu J, Nagao S, Sugahara T, et al. Die bonding performance using bimodal Cu particle paste under different sintering atmospheres. J Electron Mater 2017;46:4575–81. https://doi.org/10.1007/s11664-017-5464-2.
[22] Kobayashi Y, Abe Y, Maeda T, Yasuda Y, Morita T. A metal–metal bonding process using metallic copper nanoparticles produced by reduction of copper oxide nanoparticles. J Mater Res Technol 2014;3:114–21. https://doi.org/10.1016/j.jmrt.2013.12.003.
[23] Fujimoto T, Ogura T, Sano T, Takahashi M, Hirose A. Joining of pure copper using Cu nanoparticles derived from CuO paste. Mater Trans 2015;56:992–6. https://doi.org/10.2320/matertrans.MI201410.
[24] Zuo Y, Carter-Searjeant S, Green M, Mills L, Mannan SH. High bond strength Cu joints fabricated by rapid and pressureless in situ reduction-sintering of Cu nanoparticles. Mater Lett 2020;276:128260. https://doi.org/10.1016/j.matlet.2020.128260.
[25] Mou Y, Peng Y, Zhang Y, Cheng H, Chen M. Cu-Cu bonding enhancement at low temperature by using carboxylic acid surface-modified Cu nanoparticles. Mater Lett 2018;227:179–83. https://doi.org/10.1016/j.matlet.2018.05.037.
[26] Kobayashi Y, Shirochi T, Yasuda Y, Morita T. Preparation of metallic copper nanoparticles in aqueous solution and their bonding properties. Solid State Sci 2011;13:553–8. https://doi.org/10.1016/j.solidstatesciences.2010.12.025.
[27] Kamikoriyama Y, Imamura H, Muramatsu A, Kanie K. Ambient aqueous-phase synthesis of copper nanoparticles and nanopastes with low-temperature sintering and ultra-high bonding abilities. Sci Rep 2019;9:899. https://doi.org/10.1038/s41598-018-38422-5.
[28] Jianfeng Y, Guisheng Z, Anming H, Zhou YN. Preparation of PVP coated Cu NPS and the application for low-temperature bonding. J Mater Chem 2011;21:15981. https://doi.org/10.1039/c1jm12108a.
[29] Yan J, Zou G, Wu A, Ren J, Hu A, Zhou YN. Polymer-protected Cu-Ag mixed NPs for low-temperature bonding application. J Electron Mater 2012;41:1886–92. https://doi.org/10.1007/s11664-012-2008-7.
[30] Xiong J, Wang Y, Xue Q, Wu X. Synthesis of highly stable dispersions of nanosized copper particles using L-ascorbic acid. Green Chem 2011;13:900–4. https://doi.org/10.1039/C0GC00772B.
[31] Zhang Y, Cui C, Yang B, Zhang K, Zhu P, Li G, et al. Size-controllable copper nanomaterials for flexible printed electronics. J Mater Sci 2018;53:12988–95. https://doi.org/10.1007/s10853-018-2564-1.
[32] Choi WL, Kim YS, Lee K-S, Lee J-H. Characterization of the die-attach process via low-temperature reduction of Cu formate in air. J Mater Sci Mater Electron 2019;30:9806–13. https://doi.org/10.1007/s10854-019-01317-w.
[33] Liu J, Chen H, Ji H, Li M. Highly conductive Cu–Cu joint formation by low-temperature sintering of formic acid-treated Cu nanoparticles. ACS Appl Mater Interfaces 2016;8:33289–98. https://doi.org/10.1021/acsami.6b10280.
[34] Liu J, Ji H, Wang S, Li M. The low temperature exothermic sintering of formic acid treated Cu nanoparticles for conductive ink. J Mater Sci Mater Electron 2016;27:13280–7. https://doi.org/10.1007/s10854-016-5476-3.
[35] Gao Y, Li W, Chen C, Zhang H, Jiu J, Li C-F, et al. Novel copper particle paste with self-reduction and self-protection characteristics for die attachment of power semiconductor under a nitrogen atmosphere. Mater Des 2018;160:1265–72. https://doi.org/10.1016/j.matdes.2018.11.003.
[36] Zhao J, Yao M, Lee N-C. Nano-Cu sintering paste for high power devices die attach applications. In: 2018 IEEE 68th electronic components and technology conference (ECTC); 2018. p. 557–63. https://doi.org/10.1109/ECTC.2018.00088.
[37] Siow KS, Lin YT. Identifying the development state of sintered silver (Ag) as a bonding material in the microelectronic packaging via a patent landscape study. J Electron Packag 2016;138. https://doi.org/10.1115/1.4033069.
[38] Crisan MC, Teodora M, Lucian M. Copper nanoparticles: synthesis and characterization, physiology, toxicity and antimicrobial applications. Appl Sci 2022;12:141. https://doi.org/10.3390/app12010141.
[39] Del Carro L, Zurcher J, Drechsler U, Clark IE, Ramos G, Brunschwiler T. Low-temperature dip-based all-copper interconnects formed by pressure-assisted sintering of copper nanoparticles. IEEE Trans Compon Packag Manuf Technol 2019;9:1613–22. https://doi.org/10.1109/TCPMT.2019.2891111.
[40] Zurcher J, Carro LD, Schlottig G, Wright DN, Vardoy A-SB, Taklo MMV, et al. All-copper flip chip interconnects by pressureless and low temperature nanoparticle sintering. In: 2016 IEEE 66th electronic components and technology conference (ECTC). Las Vegas, NV, USA: IEEE; 2016. p. 343–9. https://doi.org/10.1109/ECTC.2016.42.
[41] Liu X, Zhou Q, Zhao X, Koh SW, Ye H, Zhang G. Study and application of nano copper sintering technology in power electronics packaging. In: 2021 IEEE 71st electronic components and technology conference (ECTC); 2021. p. 1928–32. https://doi.org/10.1109/ECTC32696.2021.00304.
[42] Liu X, Zhou Q, Liu Q, Tang H, Gao C, Xie B, et al. Study on the effect of mixing proportion of micro- and nano-copper particles on sintering properties. In: 2020 21st international conference on electronic packaging technology (ICEPT); 2020. p. 1–5. https://doi.org/10.1109/ICEPT50128.2020.9201937.
[43] Liu Y, Zhang H, Wang L, Fan X, Zhang G, Sun F. Effect of sintering pressure on the porosity and the shear strength of the pressure-assisted silver sintering bonding. IEEE Trans Device Mater Reliab 2018;18:240–6. https://doi.org/10.1109/TDMR.2018.2819431.
[44] Yan J, Zou G, Wu A, Ren J, Yan J, Hu A, et al. Pressureless bonding process using Ag nanoparticle paste for flexible electronics packaging. Scripta Mater 2012;66:582–5. https://doi.org/10.1016/j.scriptamat.2012.01.007.
[45] Yang F, Zhu W, Wu W, Ji H, Hang C, Li M. Microstructural evolution and degradation mechanism of SiC–Cu chip

attachment using sintered nano-ag paste during high-temperature ageing. J Alloys Compd 2020;846:156442. https://doi.org/10.1016/j.jallcom.2020.156442.
[46] Sakamoto S, Suganuma K. Thermo mechanical reliability of low-temperature low-pressure die bonding using thin Ag flake pastes. In: 2012 7th international conference on integrated power electronics systems (CIPS); 2012. p. 1–2.
[47] Zhang H, Liu Y, Wang L, Sun F, Fan J, Placette MD, et al. Effects of sintering pressure on the densification and mechanical properties of nanosilver double-side sintered power module. IEEE Trans Compon Packag Manuf Technol 2019;9:963–72. https://doi.org/10.1109/TCPMT.2018.2884032.
[48] Siow KS, Manikam VR, Chua ST. Process control of sintered Ag joint in production for die attach applications. In: Siow KS, editor. Die-attach materials for high temperature applications in microelectronics packaging. Cham: Springer International Publishing; 2019. p. 67–105. https://doi.org/10.1007/978-3-319-99256-3_3.
[49] Chen S, Zhang H. Silver sintering and soldering: bonding process and comparison. In: Siow KS, editor. Die-attach materials for high temperature applications in microelectronics packaging. Cham: Springer International Publishing; 2019. p. 1–33. https://doi.org/10.1007/978-3-319-99256-3_1.
[50] Yu F, Cui J, Zhou Z, Fang K, Johnson RW, Hamilton MC. Reliability of Ag sintering for power semiconductor die attach in high-temperature applications. IEEE Trans Power Electron 2017;32:7083–95. https://doi.org/10.1109/TPEL.2016.2631128.
[51] Fu S, Mei Y, Lu G-Q, Li X, Chen G, Chen X. Pressureless sintering of nanosilver paste at low temperature to join large area (≥100mm^2) power chips for electronic packaging. Mater Lett 2014;128:42–5. https://doi.org/10.1016/j.matlet.2014.04.127.
[52] Mou Y, Cheng H, Peng Y, Chen M. Fabrication of reliable Cu-cu joints by low temperature bonding isopropanol stabilized Cu nanoparticles in air. Mater Lett 2018;229:353–6. https://doi.org/10.1016/j.matlet.2018.07.061.
[53] Jo J-L, Anai K, Yamauchi S, Hattori T, Sakaue T. The bonding properties of various surface finishes with Cu paste for pressure sintering. In: 2020 IEEE 70th electronic components and technology conference (ECTC). Orlando, FL, USA: IEEE; 2020. p. 749–54. https://doi.org/10.1109/ECTC32862.2020.00123.
[54] Li J, Li X, Wang L, Mei Y-H, Lu G-Q. A novel multiscale silver paste for die bonding on bare copper by low-temperature pressure-free sintering in air. Mater Des 2018;140:64–72. https://doi.org/10.1016/j.matdes.2017.11.054.
[55] Chen S, Fan G, Yan X, LaBarbera C, Kresge L, Lee N-C. Achieving low-porosity sintering of nano Ag paste via pressureless process. In: 2015 IEEE 65th electronic components and technology conference (ECTC); 2015. p. 1795–802. https://doi.org/10.1109/ECTC.2015.7159842.
[56] Chen C, Zhang Z, Wang Q, Zhang B, Gao Y, Sasamura T, et al. Robust bonding and thermal-stable Ag–Au joint on ENEPIG substrate by micron-scale sinter Ag joining in low temperature pressure-less. J Alloys Compd 2020;828:154397. https://doi.org/10.1016/j.jallcom.2020.154397.
[57] Mannan S, Paknejad A, Mansourian A, Khtatba K. Morphological changes in sintered silver due to atomic migration. In: Siow KS, editor. Die-attach materials for high temperature applications in microelectronics packaging. Cham: Springer International Publishing; 2019. p. 151–63. https://doi.org/10.1007/978-3-319-99256-3_6.
[58] Wang M, Mei Y, Li X, Burgos R, Boroyevich D, Lu G-Q. How to determine surface roughness of copper substrate for robust pressureless sintered silver in air. Mater Lett 2018;228:327–30. https://doi.org/10.1016/j.matlet.2018.06.048.
[59] Gao Y, Jiu J, Chen C, Suganuma K, Sun R, Liu Z-Q. Oxidation-enhanced bonding strength of Cu sinter joints during thermal storage test. J Mater Sci Technol 2022;115:251–5. https://doi.org/10.1016/j.jmst.2021.10.047.